ACS APPLIED POLYMER MATERIALS

pubs.acs.org/acsapm
Article

Styrene-Maleic Anhydride Copolymers for High-Performance Triarylamine-Containing Electrochromic Materials

Hou-Lin Li,[§] Yu-Jen Shao,[§] Cha-Wen Chang,* and Guey-Sheng Liou*

Cite This: ACS Appl. Polym. Mater. 2024, 6, 3554−3563
Read Online

ACCESS | Metrics & More | Article Recommendations | Supporting Information

ABSTRACT: A facile approach was employed to produce thermosets of styrene-maleic anhydride copolymers (SMA) containing three kinds of triarylamine moieties to elucidate electrochromic (EC) behaviors comprehensively, and an additional ionization modification was also applied to explore the effect on counterion diffusion kinetics during the electrochemical process. The commercially available SMA was chosen as the starting material for coupling with three triarylamine-based diamine monomers, 4,4′-diamino-4″-methoxytriphenylamine (**3Ph**), *N*,*N*′-bis(4-aminophenyl)-*N*,*N*′-di(4-methoxylphenyl)-1,4-phenylenediamine (**5Ph**), and 4,4′-bis[4-aminophenyl(4-methoxyphenyl)-amino)]-4″-methoxytriphenylamine (**7Ph**), resulting in colorless and transparent thermoset polymer films with different interchain distances. Furthermore, the precursors of these polyamic acids could be reacted with triethylamine (Et_3N) to form the related triethylammonium-containing PAA complexes, which could facilitate the migration of counterion during redox procedures. After evaluating the electrochemical and EC behaviors, we demonstrate that the merge of enlarging interchain distance and ionization modifications in the triarylamine-coupling SMA copolymer matrixes leads to synergistic effects in the diffusion dynamics of the electrolyte counterion and could effectively enhance higher diffusion rates (D) of the counterion in the polymer matrix with more than 2,400 times larger (**iS5Ph**: 96.73 cm^2 $s^{-1}10^{-18}$) than the triphenylamine-based linear type polyimide, **L3Ph** (0.04 cm^2 $s^{-1}10^{-18}$), and the prepared electrochromic device (ECD) properties revealed faster coloration response speed (v_c) 43.7% s^{-1} and outstanding coloration efficiency (η_{CE}) up to 540 cm^2/C.

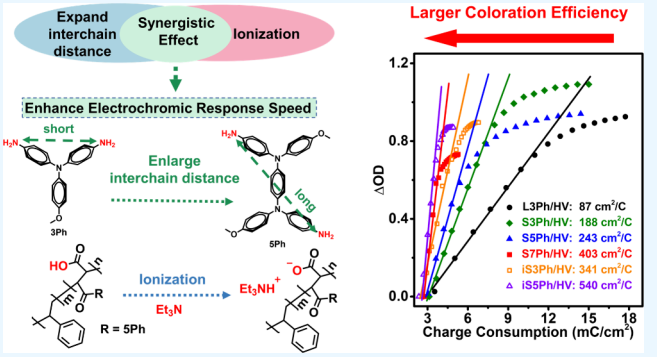

KEYWORDS: *polystyrene-maleic anhydride, triarylamine, electrochromism, cross-linking, ionization*

INTRODUCTION

Electrochromic (EC) materials reversibly change color or optical properties in response to an applied electrical voltage or current.[1] A desirable EC polymer should manifest some attractive features, including high color contrast, fast response time, swift coloring speed, significant coloration efficiency, low oxidation voltage, excellent stability, and a wide range of available colors.[1−3] Among the EC materials, triphenylamine (TPA)-based derivatives have many advantages due to their unique 3D propeller shape, such as good solubility, high transparency, and colorlessness in the neutral state. These advantages have fueled extensive research into derivatives based on triarylamines.[4−11] Recent research has demonstrated that cross-linking structures could facilitate electrolyte counterion diffusion by increasing the interchain distance within polymers,[12] and some studies have confirmed this approach of cross-linking systems, which is feasible to yield free volume, resulting in faster response capability and enhanced coloration efficiency.[13,14] This process entails the formation of covalent bonds between polymer chains, culminating in the establishment of a robust network framework. Consequently, this network imparts solvent resistance, suppresses swelling and shrinkage during redox processes, and promotes overall structural stability.[13,15,16] Abraham et al. devised small molecules containing styryl moieties to facilitate cross-linking, and the resulting films revealed exceptional solvent resistance, ensuring consistent and stable performance across more than 1500 switching cycles.[17]

Styrene-maleic anhydride (SMA) copolymer comprises styrene and maleic anhydride moieties. Despite being commercially available and cost-effective, SMA exhibits attractive performances, including excellent adhesion, thermal stability, and chemical resistance. These characteristics make it valuable for applications in which durability and reliability are essential. This copolymer has found diverse applications across

Received: February 11, 2024
Revised: February 24, 2024
Accepted: February 28, 2024
Published: March 8, 2024

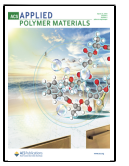

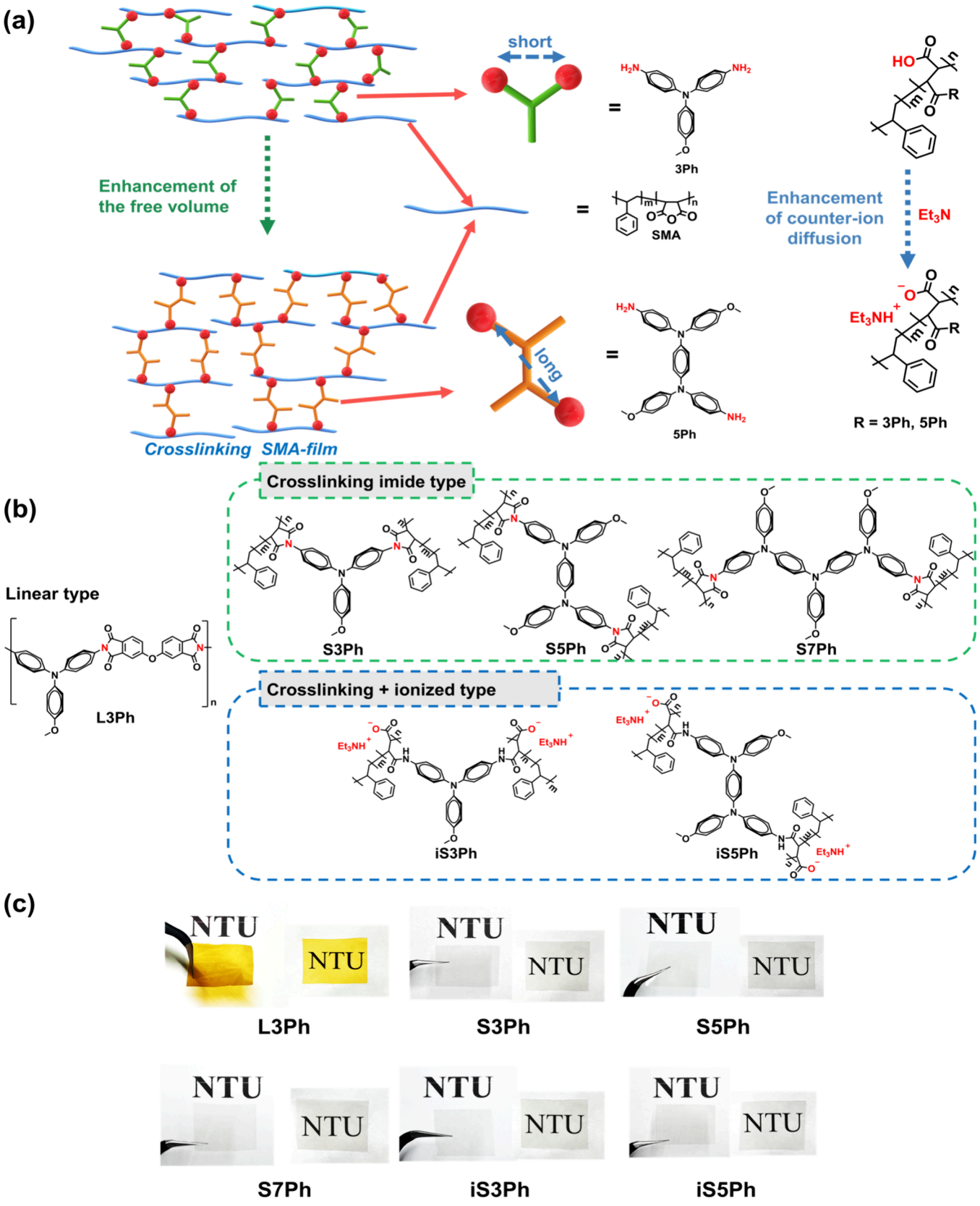

Figure 1. (a) Schematic presentation of cross-linking structures of SMA with different triarylamine linkers and (b) the target studied polymer structures in this work. (c) The photograph shows the appearance of all prepared polymer films (area: 1.5 cm × 2.0 cm; thickness: 33 ± 3 μm).

multiple domains, such as drug delivery,[18] biomedical applications,[19] dye separation,[20] and heavy metal separation.[21,22] SMA has potential advantages in different fields, but its specific benefits in optoelectronic applications have not yet been extensively explored. Some critical properties of SMA, including exceptional optical transparency, particularly within

https://doi.org/10.1021/acsapm.4c00450
ACS Appl. Polym. Mater. 2024, 6, 3554−3563

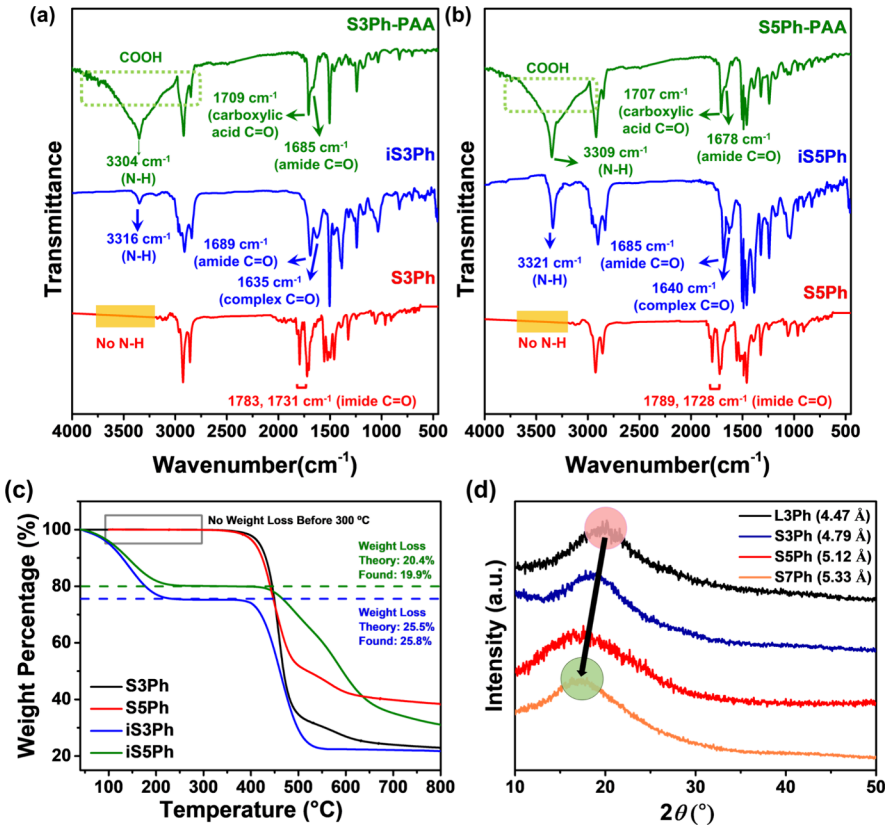

Figure 2. FT-IR spectra of (a) **3Ph** series and (b) **5Ph** series; (c) TGA curves of SMA thermosets at a 20 °C/min heating rate in a nitrogen atmosphere; (d) WXRD patterns of imide-type polymer films (thickness: 95 ± 7 μm).

the visible light range, make it have great potential and are highly suitable for transparent and colorless EC applications such as lenses, windows, and optical films, which are prime candidate areas where SMA could be utilized.

Although there has been intense research into improving the EC properties of cross-linking structures, there is still a need for a comprehensive investigation of the connection between interchain distance and electrochemical behaviors. Consequently, a facile and industrially practical approach to generating cross-linking structures of redox-active polymer films with different interchain distances is presented in this work to elucidate the relationship between interchain distance and EC properties using a series of triarylamine-based diamine cross-linkers to coupling with SMA, as shown in Figure 1. In addition, in this work, various methoxy-modified triarylamine derivatives with different molecular sizes were utilized because of their low oxidation potential and high electrochemical or electrochromic stability, according to our previous report.[23] The resulting thermoset polymers exhibited enlarged interchain distance and accelerated diffusion of the electrolyte counterion via controlling the size of triarylamine moieties. Furthermore, the ionization approach was also feasible to facilitate efficient ion transport, reduce resistance, and improve overall electrochemical efficiency.[24−28] Consequently, the ionization method was applied by using triethylamine (Et_3N) at the polyamic acid (PAA) stage to form carboxylate/triethylammonium complexes within the polymer matrix, which could substantiate faster diffusivity and enhance the EC switching response capability. Furthermore, the relationship between the interchain distance, diffusion dynamics, and electrochemical behaviors related to these two approaches was investigated systematically.

RESULTS AND DISCUSSION

2.1. Characterization and Basic Properties of the Triarylamine-Containing SMA Polymers. The diamine monomers, **3Ph**, **5Ph**, and **7Ph**, were prepared according to the previous report.[23,29,30] The detailed synthetic routes are described in the Supporting Information. The transparent and flexible polymer films could be readily prepared, as shown in Figure 1c. All the cross-linking polymer films exhibited a transparent and colorless appearance, while the structure-related linear polyimide **L3Ph** film exhibited a light yellowish appearance. The transparency of free-standing thick polymer films and thin ones applied onto ITO glasses was measured by using UV−vis spectroscopy, as illustrated in Figure S1. Remarkably, all the cross-linked SMA-derived redox-active films demonstrated excellent transparency over the visible region, leading to a colorless appearance, which could be attributed to the aliphatic backbone of SMA. Even the thick film remained highly transparent and colorless, as summarized in Figure 1c and Figure S1, manifesting it as advantageous for practical applications. FT-IR spectra carefully characterized all the synthesized polymers, as depicted in Figure 2a,b; the absorption peaks of PAA thin film observed at 3000−3500 and 3300 cm^{-1} could be ascribed to the carboxylic acid and N−H groups, respectively. Taking S3Ph-PAA as an example, after the ionization procedure, the O−H absorption peak of the carboxylic acid group disappeared. The remaining N−H peak was around 3316 cm^{-1}, and the characteristic absorption peak of the original carboxylic acid C═O also shifted from 1709 to

https://doi.org/10.1021/acsapm.4c00450
ACS Appl. Polym. Mater. 2024, 6, 3554−3563

1635 cm^{-1}, implying the formation of carboxylate. Imide-type films exhibited distinct imide absorption bands at 1783 (asymmetrical C═O) and 1731 cm^{-1} (symmetrical C═O), and the N−H group completely disappeared. The synthesis of SMA-triarylamine-coupling cross-linked polymers could be a straightforward process that could be easily accomplished by just casting the resulting polymer THF solution on the ITO glass at room temperature. After removing the solvent, the following two ways of preparation were applied: (1) heating to 160 °C for 10 h for the thermal cyclization to form polyimide type (abbreviation using "**S**" stands for cross-linking); (2) the resulting polyamic acid film without imidization procedure was immersed directly in Et_3N, which allows the formation of triethylammonium/carboxylate complex within the polymer matrix (abbreviation using "**iS**" stands for ionized and cross-linking). Detailed preparation routes for SMA-triarylamine cross-linked polymers and the ionization process are described in the Supporting Information. An additional linear TPA-based polyimide, **L3Ph**, from 4,4′-oxidiphthalic anhydride (ODPA) and **3Ph** was also prepared for comparison, according to the synthetic procedure reported in the previous literature.[23]

The thermal properties of the resulting thermosetting polymers have been measured by thermogravimetric analysis (TGA) and thermal mechanical analysis (TMA), as illustrated in Figure 2c and Figures S2 and S3 and summarized in Table S1. Liner (**L3Ph**) and imide-type polymers (**S3Ph**, **S5Ph**, and **S7Ph**) possessed remarkable thermal stability without an apparent weight loss up to 400 °C, indicating that the structures were fully transformed into imide rings. Moreover, for the ionization thermosets, Figure 2c demonstrates that the TGA of **iS3Ph** appeared to have an apparent weight loss from 60 to 220 °C, attributed to the thermal imidization. The weight loss was around 25.8%, corresponding to the theoretical weight loss of removing Et_3N and water at 24.5%. Likewise, **iS5Ph** had a weight loss value similar to the theoretical one, implying the ionic bonding formation of triethylammonium/carboxylate complexes within the polymer matrix from triethylamine and amic acid by ionization. The TMA measurements of imide-type polymers, depicted in Figure S3 and Table S1, indicate that these polymers exhibit softening temperatures (T_s) of more than 200 °C. Additionally, the values of an essential parameter in the microelectronic applications known as the coefficient of thermal expansion (CTE) for these polymers are also summarized in Table S1. The resulting SMA-based cross-linking films effectively mitigate the CTE by forming covalent bonds between molecular chains, reducing it from 70 (highest in **L3Ph**) to 50 ppm $°C^{-1}$ (lowest in **S3Ph**). This process could suppress molecular chain activity within the SMA-based polymer film, enhancing thermal performance.[31]

A Mettler Toledo scale density kit with 2,2,4-trimethylpentane as the measuring medium was used to investigate the changes in polymer densities. The densities of the polymers presented in Table S2 indicate that the cross-linking scaffold polymers (**S3Ph**: 1.213 g cm^{-3}) exhibited lower density values than the linear polymer (**L3Ph**: 1.224 g cm^{-3}), implying that the cross-linking-caused interchain distance expanding architecture generating. Furthermore, **S5Ph** (1.172 g cm^{-3}) and **S7Ph** (1.167 g cm^{-3}) also exhibited a lower density than **S3Ph**, confirming that enlarging the triarylamine plane could expand the interchain distance packing structures. To further explore the interchain distance of cross-linking polymers, wide-angle X-ray diffraction (WXRD) measurement was applied, as depicted in Figure 2d. All imide-type polymers exhibited a broad diffraction peak at approximately 18°, indicating the presence of ordered domains within the amorphous polymer matrix. The calculated *d*-spacing values from the WXRD data, as listed in Table S2, were 4.47, 4.79, 5.12, and 5.33 Å for **L3Ph**, **S3Ph**, **S5Ph**, and **S7Ph**, respectively. These values corresponded to the interchain distance between the polymer chains in the direction perpendicular to the triarylamine plane,[32] demonstrating that expanding the triarylamine plane size could produce a more significant interchain distance.

2.2. Electrochemical Properties of the Polymer Films.

The electrochemical characteristics of the polymer electrodes fabricated on ITO glasses were examined through cyclic voltammetry (CV) in a solution of 0.1 M $TBABF_4/CH_3CN$ at a scan rate of 40 mV/s. The results are illustrated in Figure 3

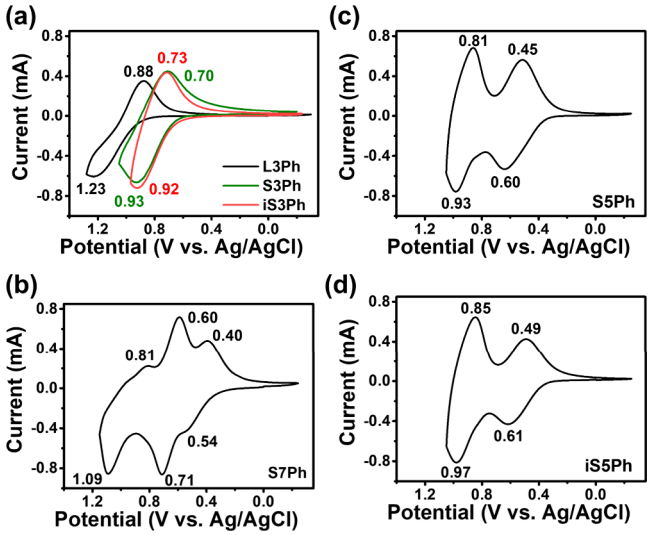

Figure 3. Cyclic voltammetry comparison of (a) **L3Ph**, **S3Ph**, and **iS3Ph** films; (b) **S7Ph**, (c) **S5Ph**, and (d) **iS5Ph** films measured on the ITO-coated glass substrate (coated area: 0.6 cm × 2 cm thickness: 340 ± 15 nm) in 0.1 M $TBABF_4/CH_3CN$ at a scan rate of 40 mV/s.

and tabulated in Table S3, and **S3Ph** (0.93 V; 0.70 V) exhibited a lower oxidation potential and ΔE compared to the linear TPA-based polyimide **L3Ph** (1.23 V; 0.88 V). The results indicate that the weak electron-withdrawing aliphatic imide ring in SMA could lower the oxidation potential, and also, the cross-linking structure facilitates the counterion migration. To confirm the impact of the cross-linking systems on counterion diffusion by the influence of expanding the size of the triarylamine plane, electrochemical impedance spectroscopy (EIS) was employed. This technique could measure resistance values consisting of electrolyte resistance (R_e), charge transfer resistance (R_{ct}), and Warburg resistance (R_W). As shown in Figure 4 and Table S3, the diameter of the semicircles in the high-frequency region represents the R_{ct} of TPA-based polymers. According to the results, the imide-type cross-linking polymers reached a lower R_{ct} to 43.5 Ω for **S3Ph** than that of **L3Ph** (45.2 Ω). In addition, along with enlarging the size of the triarylamine plane, the R_{ct} has also been lowered from 43.5 (**S3Ph**) to 38.1 Ω (**S5Ph**) and finally to the lowest value of 33.9 Ω (**S7Ph**). Furthermore, with ionization integration in cross-linking films, **iS5Ph** (34.3 Ω) resulted in more reduced R_{ct} values than **S5Ph** (38.1 Ω). Based on the literature,[33] the related ionic conductivities are calculated and

https://doi.org/10.1021/acsapm.4c00450
ACS Appl. Polym. Mater. 2024, 6, 3554−3563

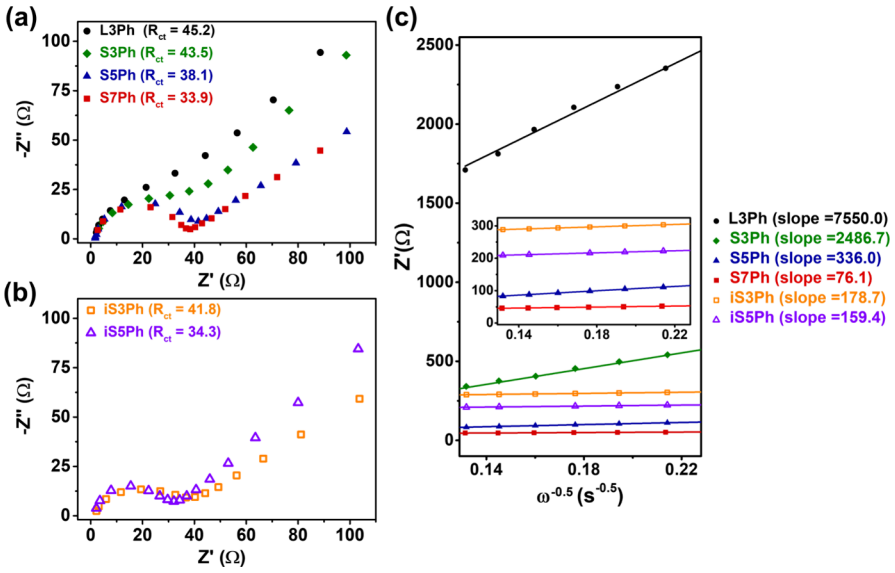

Figure 4. Nyquist plots of the prepared polymer films under the first oxidation state of (a) imide-type polymers, (b) ionized polymers, and (c) the fitted linear plot between Z′ and $\omega^{-0.5}$ in the low-frequency region.

summarized in Table S3. The imide-type cross-linking polymers reached a higher ionic conductivity of 6.51×10^{-7} S cm^{-1} for **S3Ph** than that of **L3Ph** (6.27×10^{-7} S cm^{-1}). In addition, with ionization integration in cross-linking films, **iS3Ph** (6.78×10^{-7} S cm^{-1}) resulted in an increased ionic conductivity than **S3Ph**. Similarly, **iS5Ph** (8.26×10^{-7} S cm^{-1}) also revealed a higher ionic conductivity than **S5Ph** (7.44×10^{-7} S cm^{-1}).

In addition, all six prepared polymer films displayed slope values ranging from 1 to 0.5 when plotted in a logarithm, as observed in Figures S4−S9. These slope values indicate a transitional behavior suggesting a transition between diffusion and capacitive behavior of the polymers under investigation.[34] Hence, to evaluate the diffusivity of the counterion upon the redox process, the diffusion coefficient (D) was determined by utilizing the Warburg coefficient (σ_w) within the low-frequency range in the EIS diagram.[35] The experimental outcomes are depicted and presented in Figure 4c and are summarized in Table S3. According to the results, the D value of **S3Ph** exhibited one order larger than **L3Ph**, implying that the cross-linked structure significantly promoted the counter-anions (BF_4^-) migration within the polymer matrix. Among the cross-linking polymers (**S3Ph**, **S5Ph**, and **S7Ph**), BF_4^- possessed a higher migration capability through the polymer matrix along with enlarging the triarylamine plane, resulting in smaller σ_w and a significant promotion in diffusion.[36] In addition to the increased interchain spacing, ionization could significantly enhance counterion diffusion. Some research indicates that polymers subjected to ionic complexes demonstrate heightened ionic conductivity, improving ion mobility.[28,37] The same phenomenon was also observed in this study: the ionized polymers, **iS3Ph** and **iS5Ph**, showed a considerable improvement in diffusion coefficient (D) around 192 and 4 times greater than the corresponding imide-type films, respectively, indicating that the triethylammonium/carboxylate complexes could accelerate the counterion migration. As a result, synergistic effects of interchain distance enlargement and ionization could be obtained, such that the D value of **iS5Ph** was 2,418 times greater than **L3Ph**.

2.3. Electrochromic Properties of the Polymer Films.

The electrochromic characteristics of polymer films with comparable thicknesses (340 ± 15 nm) were investigated using spectroelectrochemical spectra, as shown in Figures S10−S15. All the cross-linking polymer films at their neutral state exhibited a transparent and colorless appearance, while the **L3Ph** film exhibited a light yellowish appearance. **L3Ph**, **S3Ph**, and **iS3Ph** showed similar characteristic absorption peaks at around 370 and 780 nm when applying a positive potential to the first oxidation state, corresponding to a blue-colored appearance as depicted in Figures S10, S11, and S14, respectively. **S5Ph** and **iS5Ph** performed analogous absorption characteristics with increased absorption around 425 and 950 nm in the first oxidation state, reaching a greenish-colored appearance as demonstrated in Figures S12 and S15. The absorption in the near-infrared (NIR) region could be ascribed to intervalence charge transfer (IV-CT) resulting from the robust electron-coupling of the triarylamine cation radical.[38] Subsequently, the absorption intensity at around 820 nm escalated during the secondary oxidation process, while the original IV-CT absorption diminished. As a consequence, the film exhibited a cyan appearance.

S7Ph revealed a progressive yellowish appearance as its absorption increased at the wavelength of 430 nm and near-infrared (NIR) at 1060 nm during the first oxidation state, as shown in Figure S13. Upon applying a potential of 0.9 V (second oxidation stage), the characteristic absorbance peak at 430 nm gradually decreased, while two new bands at 540 and 1020 nm gradually increased. By further applying a positive potential was further applied to 1.2 V (third oxidation stage), the characteristic absorbance peak at 1020 nm gradually diminished, and a new band appeared at 790 nm.

A square wave potential step method was employed to observe and analyze the variation of switching response capability for the cross-linking polymer system. The coloring voltages were 1.20 V for **L3Ph**, 0.95 V for **S3Ph** and **iS3Ph**, and 0.70 V for **S5Ph**, **iS5Ph**, and **S7Ph**, while the bleaching voltages were −0.2 V for all the devices. The response time denotes the duration of the EC materials required to achieve 90% of the saturated absorption change, as observed through

https://doi.org/10.1021/acsapm.4c00450
ACS Appl. Polym. Mater. 2024, 6, 3554−3563

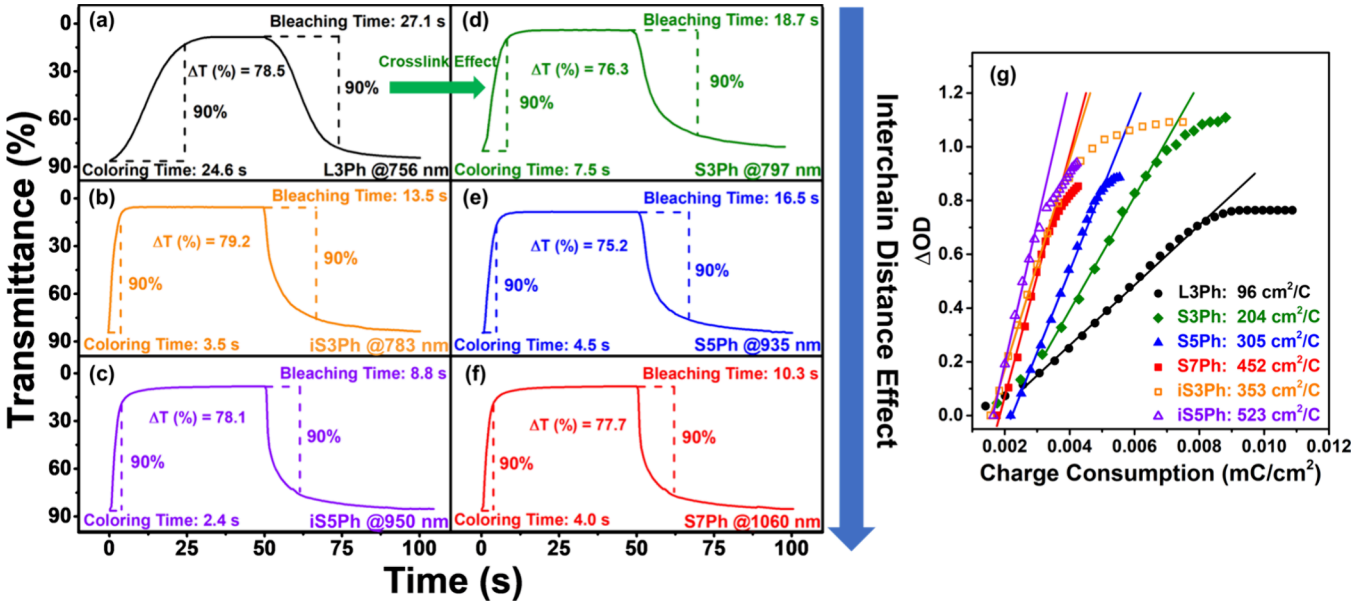

Figure 5. Switching response time of (a) **L3Ph**, (b) **iS3Ph**, (c) **iS5Ph**, (d) **S3Ph**, (e) **S5Ph**, and (f) **S7Ph** films; (g) η_{CE} of prepared films on the ITO-coated glass substrate (coated area: 0.6 cm × 2 cm; thickness: 340 ± 15 nm) in 0.1 M $TBABF_4/CH_3CN$. The coloring voltages were 1.20 V for **L3Ph**, 0.95 V for **S3Ph**, and **iS3Ph**, 0.70 V for **S5Ph**, **iS5Ph**, and **S7Ph**, while the bleaching voltages were −0.2 V for all the devices.

absorbance measurements at a specific wavelength, indicated in Figure 5 and Table S4. The imide-type cross-linking film, **S3Ph**, exhibited shorter response times at coloring t_c (7.5 s) and bleaching t_b (18.7 s) states compared to the linear polymer film, **L3Ph** (t_c: 24.6 s; t_b: 27.1 s). In addition, the interchain distance also exhibited a crucial influence; from the shortest **S3Ph** (t_c: 7.5 s; t_b: 18.7 s) to **S5Ph** (t_c: 4.5 s; t_b: 16.5 s) to the longest **S7Ph** (t_c: 4.0 s; t_b: 10.3 s), both t_c and t_b have been significantly improved. Compared to the effect of increasing the interchain distance, the ionized polymers exhibited an even superior enhancement. As shown in Figure 5, **iS3Ph** (t_c: 3.5 s; t_b: 13.5 s) and **iS5Ph** (t_c: 2.4 s; t_b: 8.8 s) revealed 37 and 47% response time reduction to the corresponding imide-type film, respectively. Besides promoting the response capabilities, the coloration efficiency (η_{CE}) and response speed (υ_c) were also effectively enhanced. From the smallest interchain distance **S3Ph** (η_{CE}: 204 $cm^2\ C^{-1}$; υ_c: 9.2% s^{-1}) to **S5Ph** (η_{CE}: 305 $cm^2\ C^{-1}$; υ_c: 15.0% s^{-1}) and to the largest **S7Ph** (η_{CE}: 452 $cm^2\ C^{-1}$; υ_c: 17.5% s^{-1}), the η_{CE} and υ_c could be increased as shown in Table S4. The ionized films of **iS3Ph** (η_{CE}: 353 $cm^2\ C^{-1}$; υ_c: 20.4% s^{-1}) and **iS5Ph** (η_{CE}: 523 $cm^2\ C^{-1}$; υ_c: 29.3% s^{-1}) exhibited a sharper and lower amount of ejecting charge during the oxidation or reduction process and ultimately revealed both the highest η_{CE} and υ_c.

2.4. Electrochromic Properties of the Prepared ECDs. The corresponding electrochromic devices (ECDs) have been prepared to explore further practical demonstration. The ECDs were subjected to an electrolyte solution injection comprising 165 mg (0.1 M) of $TBABF_4$, 80 mg (30 μM) of heptyl viologen (HV), and 10 wt % of PMMA in a 5 mL volume of propylene carbonate (PC). Viologen-based derivatives are a widely studied EC material,[39] and the previous research has indicated that the presence of HV could enhance the redox stability of ECDs, as HV^{2+} could accept electrons from triarylamine during oxidation, resulting in the conversion to HV^{+} and a subsequent reduction in the applied voltage window.[40] It is postulated that ECDs incorporating HV could lower oxidation potentials and accelerate the switching response capability. Consequently, CV measurements were employed to elucidate the electrochemical behavior, as illustrated in Figure S16 and Table S5. The obtained results indicated a consistent conclusion with those of the individual films, wherein a reduced ΔE value from a more significant chain distance extending film of **S7Ph/HV** (0.18 V) to an ionized film of **iS5Ph/HV** (0.14 V) when compared with **L3Ph/HV** (0.35 V).

The spectroelectrochemical spectra of the ECDs with a comparable thickness of polymer films, approximately 210 ± 10 nm, were used to investigate the electrochromic characteristics, as depicted in Figure 6. The cross-linking SMA-based ECDs displayed a transparent and colorless feature at the neutral state. In contrast, the EC behavior revealed slightly different from the film-type ones during the oxidation state because of the participation of HV. According to the spectroelectrochemical spectra, in addition to the new two absorptions contributed by HV, which showed up at 400 and 605 nm, the characteristic absorption of all others remained the same. Thus, the ECDs appeared more intensive deep blue during oxidation by benefiting from these two new absorptions. The CIELAB color space parameters were adopted to measure the color transformation of the ECDs throughout the redox process. The device appearance and the corresponding $L^*a^*b^*$ values are summarized in Figure 6. With the cooperation of **HV**, the absorption window of cross-linking SMA-based polymers could be perfectly complemented to give a higher contrast. Thus, the device fabricated from **S3Ph/HV** exhibited a transparent and colorless appearance at the neutral state (L^*: 97.61, a^*: −1.55, b^*: 3.95) and changed to a deep-blue appearance (L^*: 41.95, a^*: −7.66, b^*: −48.90) after oxidation at 1.3 V. A similar color change could be observed for the other structure-related **3Ph/HV** series ECD. For **S5Ph/HV**, the color could change from colorless (L^*: 98.43, a^*: −1.95, b^*: 3.33) to cyan (L^*: 58.24, a^*: −24.81, b^*: −3.62) and then deeper blue (L^*: 40.11, a^*: −15.08, b^*: −41.22), and a similar color change could also be obtained for **iS5Ph/HV** ECD. Then, the device based on **S7Ph/HV**

https://doi.org/10.1021/acsapm.4c00450
ACS Appl. Polym. Mater. 2024, 6, 3554−3563

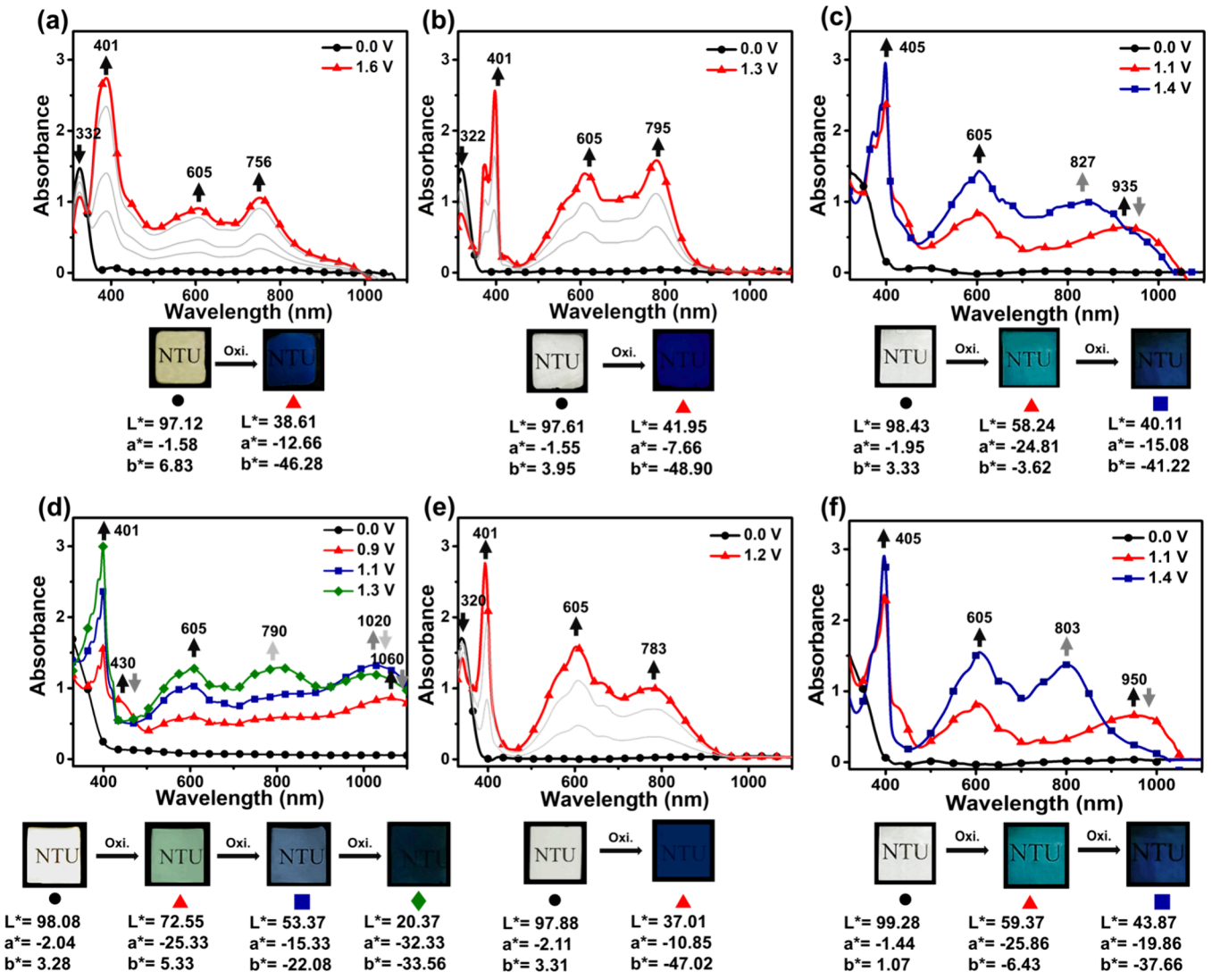

Figure 6. Spectroelectrochemistry diagrams of (a) **L3Ph/HV**, (b) **S3Ph/HV**, (c) **S5Ph/HV**, (d) **S7Ph/HV**, (e) **iS3Ph/HV**, and (f) **iS5Ph/HV**; the devices were fabricated on ITO glass with a 2 cm × 2 cm active area containing 0.03 M of HV and 0.1 M of $TBABF_4$ as the supporting electrolyte in 0.05 mL PC with 10 wt % PMMA (polymer film 210 ± 15 nm in thickness). The appearance of the ECDs and CIELAB parameters is also presented.

displayed color changes from colorless and transparent (L^*: 98.08, a^*: −2.04, b^*: 3.28) to mint green (L^*: 72.55, a^*: −25.33, b^*: 5.33), then sky blue (L^*: 53.37, a^*: −15.33, b^*: −22.08), and finally, deeper blue (L^*: 20.37, a^*: −32.33, b^*: −33.56) related to the different oxidation states.

Furthermore, the crucial properties of switching response capability and redox stability for the resulted ECDs in this study were investigated by using a square wave potential step method between 1.3 V for **L3Ph/HV**, 1.1 V for **S3Ph/HV**, and **iS3Ph/HV**, 1.0 V for **S5Ph/HV**, **S7Ph/HV**, and **iS5Ph/HV** as coloring voltage and −0.3 V as bleaching voltage. According to the results from Figure 7 and Table S6, the ECDs revealed the same trend as the single film, with increasingly more considerate interchain distances demonstrating a shorter response time in t_c or t_b than those with smaller interchain spaces. For example, **S5Ph/HV**, compared to the **S3Ph/HV**, exhibited a shorter response time of 3.8 s in the coloring and 9.7 s in the bleaching processes, and **S7Ph/HV** revealed an even quicker response time of 2.7 and 6.6 s in the same switching and bleaching processes, respectively.

Additionally, the judicious inclusion of the redox-active cross-linking scaffold within the SMA-based ECDs could not only decrease the switching times between the neutral and colored states but also considerably enhance the electrochemical stability of the resulting ECD, as demonstrated in Figure 8 and Figure S17 from **L3Ph/HV** (72% for 1000 cycles) to **S3Ph/HV** (88% for 1000 cycles), **S5Ph/HV** (93% for 1000 cycles), and **S7Ph/HV** (97% for 1000 cycles). Besides enlarging the interchain distance, the ionization approach could be even more influential in enhancing ECD behaviors. After ionization, **iS3Ph/HV** and **iS5Ph/HV** showed a considerable improvement in response time, taking only 2.5 and 1.7 s in the coloring process, respectively. Synergistic effects of interchain distance enlargement and ionization could be achieved when merging these two advantageous approaches; the υ_c of **iS5Ph/HV** (43.7% s^{-1}) was accomplished to be 3 times faster than **S3Ph/HV** (13.3% s^{-1}), and accompanied a high η_{CE} value of 540 cm^2/C. Due to the cross-linking scaffold effect, ionization film also could present

https://doi.org/10.1021/acsapm.4c00450
ACS Appl. Polym. Mater. 2024, 6, 3554−3563

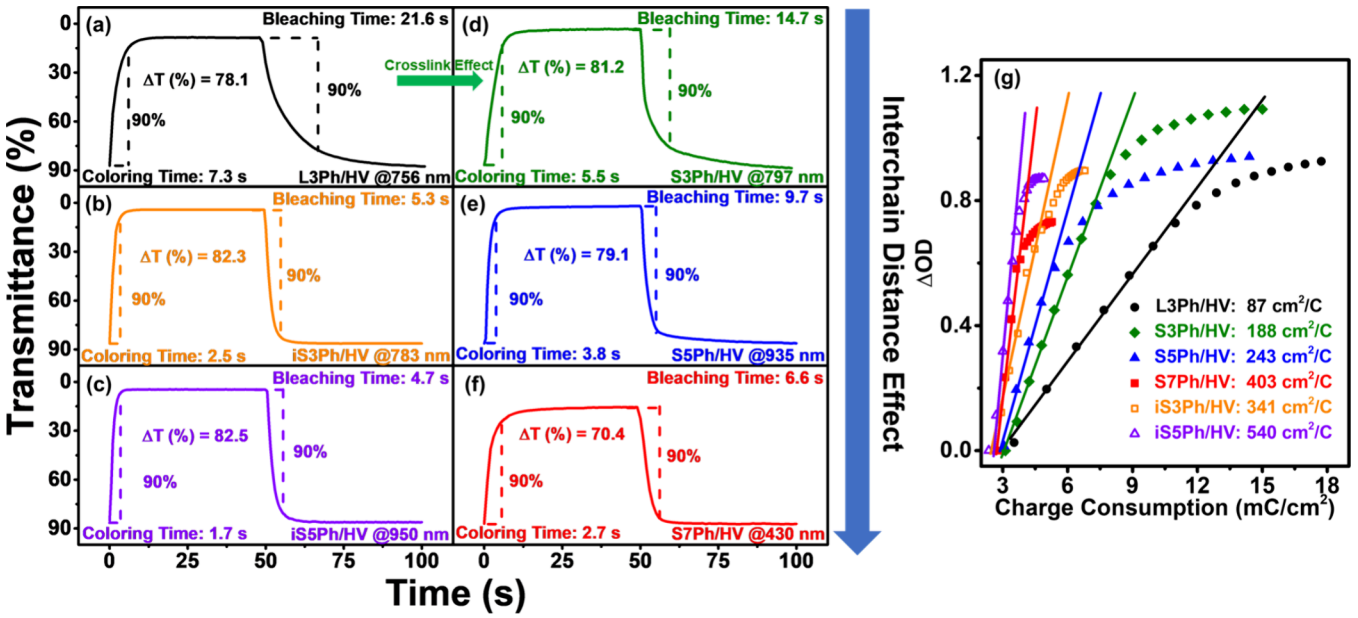

Figure 7. Switching response time of (a) **L3Ph/HV**, (b) **iS3Ph/HV**, (c) **iS5Ph/HV**, (d) **S3Ph/HV**, (e) **S5Ph/HV**, and (f) **S7Ph/HV**; (g) η_{CE} of ECDs with 2 cm × 2 cm active area containing 0.03 M of HV and 0.1 M of $TBABF_4$ as the supporting electrolyte in 0.05 mL PC with 10 wt % of PMMA (polymer film 210 ± 15 nm in thickness). The coloring voltages were 1.3 V for **L3Ph/HV**, 1.1 V for **S3Ph/HV**, and **iS3Ph/HV**, 1.0 V for **S5Ph/HV**, **iS5Ph/HV**, and **S7Ph/HV**, while the bleaching voltages were −0.3 V for all of the devices.

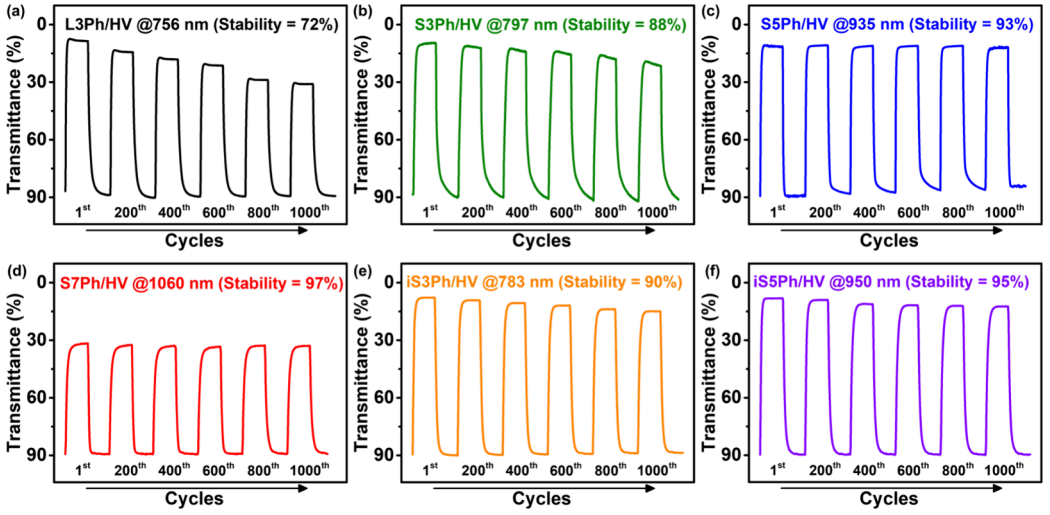

Figure 8. EC repetitive switching stability of (a) **L3Ph/HV**, (b) **S3Ph/HV**, (c) **S5Ph/HV**, (d) **S7Ph/HV**, (e) **iS3Ph/HV**, and (f) **iS5Ph/HV** for 1000 cycles, 1.1 V for **L3Ph/HV**, **S3Ph/HV**, and **iS3Ph/HV**, 1 V for **S5Ph/HV**, **iS5Ph/HV**, and **S7Ph/HV** (in the ON state), and all the OFF states at −0.3 V with 2 cm × 2 cm active area containing 0.03 M of HV and 0.1 M of $TBABF_4$ as the supporting electrolyte in 0.05 mL PC with 10 wt % PMMA (polymer film 210 ± 10 nm in thickness).

outstanding stability, **iS3Ph/HV** (90% for 1000 cycles) and **iS5Ph/HV** (95% for 1000 cycles).

CONCLUSIONS

This study systematically investigated a series of SMA-based triarylamine-coupling redox-active polymers to elucidate the impact of expanding the interchain distance and ionization modification on the EC behaviors of the resulting polymer films. The cross-linking imide-type polymer of **S7Ph** showed a much larger *d*-spacing of 5.33 Å and a lower density of 1.167 g cm^{-3} compared to the related linear polyimide (**L3Ph**) with a *d*-spacing of 4.47 Å and density of 1.224 g cm^{-3}, suggesting that the cross-linking approach could effectively enlarge the interchain distance between polymer chains, leading to an increasing amount of space within the polymer matrix. According to electrochemical and EC measurement results, either the enlargement of the triarylamine plane or the ionization method could effectively improve the electrochemical properties and EC performances, individually, such as the reduced ΔE (**L3Ph**: 0.35 V; **S7Ph**: 0.14 V; **iS5Ph**: 0.12 V), shorter coloring time t_c (**L3Ph**: 24.6 s; **S7Ph**: 4.0 s; **iS5Ph**: 2.4 s), enhanced response speed efficiency υ_c (**L3Ph**: 2.9% s^{-1}; **S7Ph**: 17.5% s^{-1}; **iS5Ph**: 29.3% s^{-1}), and higher coloring efficiency η_{CE} (**L3Ph**: 96 cm^2/C; **S7Ph**: 452 cm^2/C; **iS5Ph**: 523 cm^2/C). Intriguingly, merging these two approaches demonstrated a synergistic effect and brought out the most admirable material of **iS5Ph**, which exhibited the shortest response time (t_c: 2.4 s; t_b: 8.8 s) and the highest υ_c (29.3%

https://doi.org/10.1021/acsapm.4c00450
ACS Appl. Polym. Mater. 2024, 6, 3554−3563

s^{-1}) and η_{CE} (523 cm^2/C). In the evaluation of ECDs, the trend of improvements in electrochemical and electrochromic behaviors was similar to the pristine film analyses. Among all series, **iS5Ph/HV** revealed a synergistic effect, leading to the shortest t_c (1.7 s), highest υ_c (43.7%s^{-1}) and η_{CE} (540 cm^2/C), and exceptional stability up to 95% over 1000 cycles, manifesting it the most fabulous ECD in this study. These findings highlight the significant impact on the feasibility of utilizing the commercially available and cost-competitive SMA as an optoelectronic material by the facile approaches of enlarging the interchain distance and implementing ionization modification on the EC performance of the resulting SMA-based cross-linking polymers.

EXPERIMENTAL SECTION/METHODS

Materials. 4,4′-Diamino-4″-methoxytriphenylamine (**3Ph**),[23] *N*,*N*′-bis(4-aminophenyl)-*N*,*N*′-di(4-methoxylphenyl)-1,4-phenylenediamine (**5Ph**),[30] 4,4′-bis[4-aminophenyl(4-methoxyphenyl)amino)]-4″-methoxytriphenylamine (**7Ph**),[29] and heptyl viologen tetrafluoroborate (**HV**)[41] were synthesized according to the previous reports. The following steps prepared tetrabutylammonium tetrafluoroborate (**TBABF$_4$**): the aqueous tetrabutylammonium bromide (**TBABr**) was added into the saturated solution of sodium tetrafluoroborate (**NaBF$_4$**) in DI water under vigorous stirring. Afterward, the obtained white precipitate was recrystallized with a 2:1 water/ethanol solution. Other materials such as 4-bromoanisole (Alfa), 4,4′-oxydiphthalic anhydride (TCI), potassium carbonate (Alfa), SMA (SMA 1000) (Cray Valley), triethylamine (Et_3N) (Thermofisher), copper powder (Acros), 18-crown-6 ether (TCI), PMMA, hydrazine monohydrate (Alfa), palladium on activated charcoal (Pd/C) (Acros), tetrabutylammonium perchlorate (TBAP) (Alfa), and all of the solvent were used as received from commercial sources.

Synthesis of SMA-Based-Cross-Linking Polymers. The synthesis of polymers **S3Ph** is used as an example to illustrate the general synthetic route. The typical procedure was as follows: a mixture of **3Ph** (0.1644 g, 0.125 mmol) and **SMA** (0.2500 g, 0.125 mmol) in 4 mL of THF was stirred at room temperature for 2 h. After 2 h, the triethylamine (Et_3N) was slowly dripped into the mixture. Then, the polymer solution was diluted to 2 mg/mL of DMF and drop-coated onto the 3 cm × 2.5 cm ITO-coated glassy substrate in the vacuum oven. After dropping on the ITO glass, most of the solvent was removed in the vacuum oven at 50 °C. Then, the temperature was raised to 120 °C for 2 h and 160 °C for 10 h in a vacuum for the thermal imidization and forming of the resulting polyimide film.

Synthesis of Ionized-Cross-Linking Polymers. The synthesis of polymer **iS3Ph** is an example to illustrate the general synthetic route. The typical procedure was as follows: a mixture of **3Ph** (0.1644 g, 0.125 mmol) and **SMA** (0.2500 g, 0.125 mmol) in 4 mL of THF was stirred at room temperature for 2 h. Then, the polymer solution was diluted to 2 mg/mL of DMF and drop-coated onto the 3 cm × 2.5 cm ITO-coated glassy substrate in the vacuum oven to remove most of the solvent to obtain the resulting polymer film. Afterward, the film was immersed in Et_3N for 15 min for ionization and then dipped in MeCN for 5 min three times to remove excess Et_3N.

ASSOCIATED CONTENT

Supporting Information

The Supporting Information is available free of charge at https://pubs.acs.org/doi/10.1021/acsapm.4c00450.

Measurement section, preparation section (including polymeric film and ECDs preparation), UV−vis spectra, thermal properties, cyclic voltammetric diagrams, and spectroelectrochemical diagrams (PDF)

AUTHOR INFORMATION

Corresponding Authors

Cha-Wen Chang − *Department of Digital Printing Materials, Division of Applied Chemistry Material and Chemical Research Laboratories, Industrial Technology Research Institute, Hsinchu 300044, Taiwan*; Email: ChaWen@itri.org.tw

Guey-Sheng Liou − *Institute of Polymer Science and Engineering, National Taiwan University, Taipei 10617, Taiwan*; orcid.org/0000-0003-3725-3768; Email: gsliou@ntu.edu.tw

Authors

Hou-Lin Li − *Institute of Polymer Science and Engineering, National Taiwan University, Taipei 10617, Taiwan*

Yu-Jen Shao − *Institute of Polymer Science and Engineering, National Taiwan University, Taipei 10617, Taiwan*

Complete contact information is available at: https://pubs.acs.org/10.1021/acsapm.4c00450

Author Contributions

[§]H.L.L. and Y.J.S. contributed equally to this paper.

Notes

The authors declare no competing financial interest.

ACKNOWLEDGMENTS

This work received financial support from the National Science and Technology Council in Taiwan (NSTC 111-2113-M-002-024 and 111-2221-E-002-028-MY3).

REFERENCES

(1) Mortimer, R. J.; Dyer, A. L.; Reynolds, J. R. Electrochromic organic and polymeric materials for display applications. *Displays* **2006**, *27* (1), 2−18.

(2) Tsuboi, A.; Nakamura, K.; Kobayashi, N. Multicolor electrochromism showing three primary color states (cyan−magenta−yellow) based on size-and shape-controlled silver nanoparticles. *Chem. Mater.* **2014**, *26* (22), 6477−6485.

(3) Li, X.; Wang, Z.; Chen, K.; Zemlyanov, D. Y.; You, L.; Mei, J. Stabilizing hybrid electrochromic devices through pairing electrochromic polymers with minimally color-changing ion-storage materials having closely matched electroactive voltage windows. *ACS Appl. Mater. Interfaces* **2021**, *13* (4), 5312−5318.

(4) Hao, Q.; Li, Z. J.; Lu, C.; Sun, B.; Zhong, Y. W.; Wan, L. J.; Wang, D. Oriented two-dimensional covalent organic framework films for near-infrared electrochromic application. *J. Am. Chem. Soc.* **2019**, *141* (50), 19831−19838.

(5) Ma, Y.; Xia, S.; Zhai, M.; Zhang, C.; Hong, T.; Zhang, B.; Cai, W.; Niu, H.; Wang, W. Non-planar polyimides with monomer containing four triphenylamines for near-infrared electrochromism and TNP detection. *J. Appl. Polym. Sci.* **2023**, *140* (36), No. e54377.

(6) Kim, K. W.; Lee, J. K.; Tang, X.; Lee, Y.; Yeo, J.; Moon, H. C.; Lee, S. W.; Kim, S. H. Novel triphenylamine containing poly-viologen for voltage-tunable multi-color electrochromic device. *Dyes Pigm.* **2021**, *190*, No. 109321.

(7) Feng, F.; Sun, N.; Wang, D.; Zhou, H.; Chen, C. A series of organosoluble polyamides with 4-(dimethylamino) triphenylamine: synthesis, thermal and electrochromic properties. *High Perform. Polym.* **2017**, *29* (8), 922−930.

(8) Rusu, R. D.; Damaceanu, M. D.; Ursache, S.; Constantin, C. P. Tuning the main electrochromic features by polymer backbone variation of triphenylamine-based polyamides. *J. Photochem. Photobiol., A* **2023**, *435*, No. 114272.

(9) Huang, Q.; Chen, J.; Shao, X.; Zhang, L.; Dong, Y.; Li, W.; Zhang, C.; Ma, Y. New electropolymerized triphenylamine polymer

films and excellent multifunctional electrochromic energy storage system materials with real-time monitoring of energy storage status. *Chemical Engineering Journal* **2023**, *461*, No. 141974.
(10) Yu, T.; Theato, P.; Yao, H.; Liu, H.; Di, Y.; Sun, Z.; Guan, S. Colorless electrochromic/electrofluorochromic dual-functional triphenylamine-based polyimides: Effect of a tetraphenylethylene-based π-bridge on optoelectronic properties. *Chemical Engineering Journal* **2023**, *451*, No. 138441.
(11) Lv, X.; Shao, M.; Zhu, X.; Xu, L.; Ouyang, M.; Zhou, C.; Dong, J.; Zhang, C. Thermally crosslinked copolymer for highly transparent to multicolor-showing electrochromic materials. *ACS Applied Polymer Materials* **2023**, *5* (5), 3595−3603.
(12) Lv, X.; Li, J.; Xu, L.; Zhu, X.; Tameev, A.; Nekrasov, A.; Kim, G.; Xu, H.; Zhang, C. Colorless to multicolored, fast switching, and highly stable electrochromic devices based on thermally crosslinking copolymer. *ACS Appl. Mater. Interfaces* **2021**, *13* (35), 41826−41835.
(13) Sun, Y.; Zhu, G.; Zhao, X.; Kang, W.; Li, M.; Zhang, X.; Yang, H.; Guo, L.; Lin, B. Solution-processable, hypercrosslinked polymer via post-crosslinking for electrochromic supercapacitor with outstanding electrochemical stability. *Sol. Energy Mater. Sol. Cells* **2020**, *215*, No. 110661.
(14) Balakrishnan, S.; Venugopal, R.; Harikumar, A.; Deb, B.; Joseph, J. Effect of hyper-cross-linking on the electrochromic device properties of cross-linkable carbazole−diphenylamine derivatives. *ACS Applied Polymer Materials* **2023**, *5* (6), 4170−4179.
(15) Li, T.; Liu, P.; Gao, Y.; Diao, S.; Wang, X.; Yang, B.; Wang, X. High electrochemical performance of supercapacitor electrode with *para*-aminophenyl graphene/polyaniline crosslinking nanocomposites. *Mater. Lett.* **2019**, *244*, 13−17.
(16) Chen, K.; Wu, Y.; You, L.; Wu, W.; Wang, X.; Zhang, D.; Elman, J. F.; Ahmed, M.; Wang, H.; Zhao, K.; Mei, J. Printing dynamic color palettes and layered textures through modeling-guided stacking of electrochromic polymers. *Mater. Horiz.* **2022**, *9* (1), 425−432.
(17) Abraham, S.; Mangalath, S.; Sasikumar, D.; Joseph, J. Transmissive-to-black electrochromic devices based on cross-linkable tetraphenylethene-diphenylamine derivatives. *Chem. Mater.* **2017**, *29* (23), 9877−9881.
(18) Ball, L. E.; Pfukwa, R.; Siqueira, R. P.; Mosqueira, V. C. F.; Klumperman, B. PLA-*b*-SMA as an amphiphilic diblock copolymer for encapsulation of lipophilic cargo. *Macromol. Chem. Phys.* **2023**, *224* (1), 2200212.
(19) Almehizia, A. A.; Alkahtani, H. M.; Al-Omar, M. A.; Obaidullah, A. J.; Bhat, M. A.; Alrasheed, L. S.; Naglah, A. M.; Younes, A. A. O.; Alsuhaibani, A. M.; Refat, M. S.; Adam, A. M. A.; El-Sayed, M. Y.; Asla, K. A. Synthesis, spectroscopic characterization and thermal studies of polymer-metal complexes derived from modified poly styrene-*alt*-(maleic anhydride) as a prospects for biomedical applications. *Crystals* **2023**, *13* (5), 728.
(20) Luo, Q.; Shao, H.; Chang, J.; Diao, Y.; Zhang, F.; Qin, S. One-step fabrication of robust polyvinyl chloride loose nanofiltration membranes by synthesizing a novel polyether amine grafted styrene-maleic anhydride copolymer. *Sep. Purif. Technol.* **2023**, *309*, No. 123033.
(21) Hasanzadeh, R.; Najafi Moghadam, P.; Samadi, N. Synthesis and application of modified poly (styrene-*alt*-maleic anhydride) networks as a nano chelating resin for uptake of heavy metal ions. *Polym. Adv. Technol.* **2013**, *24* (1), 34−41.
(22) Yang, Y.; Wang, S.; Zhang, J.; He, B.; Li, J.; Qin, S.; Yang, J.; Zhang, J.; Cui, Z. Fabrication of hollow fiber nanofiltration separation layer with highly positively charged surface for heavy metal ion removal. *J. Membr. Sci.* **2022**, *653*, No. 120534.
(23) Chang, C. W.; Liou, G. S.; Hsiao, S. H. Highly stable anodic green electrochromic aromatic polyamides: synthesis and electrochromic properties. *J. Mater. Chem.* **2007**, *17* (10), 1007−1015.
(24) Yang, Z.; Zhong, J.; Feng, J.; Li, J.; Kang, F. Highly reversible anion redox of manganese-based cathode material realized by electrochemical ion exchange for lithium-ion batteries. *Adv. Funct. Mater.* **2021**, *31* (48), 2103594.
(25) Ko, W.; Kim, J.; Kang, J.; Park, H.; Lee, Y.; Ahn, J.; Ku, B.; Choi, M.; Ahn, H.; Oh, G.; Hwang, J. Y.; Kim, J. Development of P3-type $K_{0.70}[Cr_{0.86}Sb_{0.14}]O_2$ cathode for high-performance K-ion batteries. *Mater. Today Energy* **2023**, *36*, No. 101356.
(26) Wang, J.; Zhang, L.; Hu, Y.; Du, X.; Hao, X.; Cao, Q.; Guan, G.; Liu, Z.; Li, J.; Luo, S.; An, X. Intrinsic facet-dependent electrochemical activities of BiOBr nanosheets for Br-exchange in electrochemically switched ion exchange process. *Chem. Eng. J.* **2023**, *460*, No. 141798.
(27) Kim, H.; Byeon, Y. W.; Wang, J.; Zhang, Y.; Scott, M. C.; Jun, K.; Cai, Z.; Sun, Y. Understanding of electrochemical K^+/Na^+ exchange mechanisms in layered oxides. *Energy Storage Materials* **2022**, *47*, 105−112.
(28) Kim, Y. M.; Choi, W. Y.; Kwon, J. H.; Lee, J. K.; Moon, H. C. Functional ion gels: versatile electrolyte platforms for electrochemical applications. *Chem. Mater.* **2021**, *33* (8), 2683−2705.
(29) Liou, G. S.; Lin, H. Y. Synthesis and electrochemical properties of novel aromatic poly (amine−amide)s with anodically highly stable yellow and blue electrochromic behaviors. *Macromolecules* **2009**, *42* (1), 125−134.
(30) Yen, H. J.; Liou, G. S. Solution-processable novel near-infrared electrochromic aromatic polyamides based on electroactive tetraphenyl-*p*-phenylenediamine moieties. *Chem. Mater.* **2009**, *21* (17), 4062−4070.
(31) Jiao, L.; Luo, F.; Du, Z.; Dai, X.; Mu, J.; Wang, H.; Dong, Z.; Qiu, X. Ultra-high T_g and ultra-low CTE polyimide films based on tunable interchain crosslinking. *React. Funct. Polym.* **2022**, *181*, No. 105449.
(32) Zhuang, Y.; Seong, J. G.; Do, Y. S.; Jo, H. J.; Cui, Z.; Lee, J.; Lee, Y. M.; Guiver, M. D. Intrinsically microporous soluble polyimides incorporating Tröger's base for membrane gas separation. *Macromolecules* **2014**, *47* (10), 3254−3262.
(33) Constantin, C. P.; Balan-Porcarasu, M.; Lisa, G. Exploring innovative synthetic solutions for advanced polymer-based electrochromic energy storage devices: Phenoxazine as a promising chromophore. *Journal of Energy Chemistry* **2024**, *91*, 433−452.
(34) Chodankar, N. R.; Pham, H. D.; Nanjundan, A. K.; Fernando, J. F.; Jayaramulu, K.; Golberg, D.; Han, Y. K.; Dubal, D. P. True meaning of pseudocapacitors and their performance metrics: asymmetric versus hybrid supercapacitors. *Small* **2020**, *16* (37), 2002806.
(35) Lv, X.; Yan, S.; Dai, Y.; Ouyang, M.; Yang, Y.; Yu, P.; Zhang, C. Ion diffusion and electrochromic performance of poly (4, 4', 4"-tris [4-(2-bithienyl) phenyl] amine) based on ionic liquid as electrolyte. *Electrochim. Acta* **2015**, *186*, 85−94.
(36) Chiu, Y.; Tan, W. S.; Yang, J.; Pai, M.; Liou, G. Electrochromic response capability enhancement with pentiptycene-incorporated intrinsic porous polyamide films. *Macromol. Rapid Commun.* **2020**, *41* (12), 2000186.
(37) Ngai, K. S.; Ramesh, S.; Ramesh, K.; Juan, J. C. A review of polymer electrolytes: fundamental, approaches and applications. *Ionics* **2016**, *22*, 1259−1279.
(38) Yen, H. J.; Liou, G. S. Recent advances in triphenylamine-based electrochromic derivatives and polymers. *Polym. Chem.* **2018**, *9* (22), 3001−3018.
(39) Yu, K. S.; Kim, S. Y.; Moon, H. C. High-voltage pulse-assisted operation of single-layer electrochromic systems for high performance and reliability. *ACS Appl. Mater. Interfaces* **2023**, *15* (38), 45315−45321.
(40) Liu, H. S.; Pan, B. C.; Liou, G. S. Highly transparent AgNW/PDMS stretchable electrodes for elastomeric electrochromic devices. *Nanoscale* **2017**, *9* (7), 2633−2639.
(41) Lu, H. C.; Kao, S. Y.; Yu, H. F.; Chang, T. H.; Kung, C. W.; Ho, K. C. Achieving low-energy driven viologens-based electrochromic devices utilizing polymeric ionic liquids. *ACS Appl. Mater. Interfaces* **2016**, *8* (44), 30351−30361.

https://doi.org/10.1021/acsapm.4c00450
ACS Appl. Polym. Mater. 2024, 6, 3554−3563